

Doctoral Dissertation

Study on the Improvement of Perovskite Solar Cell Efficiency

Trinh Xuan Long

Department of Mechanical Engineering

Graduate School, Inje University

Advisor: Prof. HyunChul Kim

Study on the Improvement of Perovskite Solar Cell Efficiency

Trinh Xuan Long

Department of Mechanical Engineering

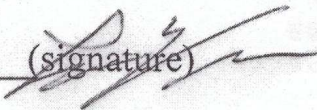
Graduate School, Inje University

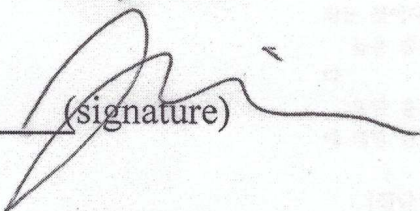
A thesis submitted to the Graduate School of Inje
University in partial fulfillment of the requirements for
the degree of Doctor of Engineering

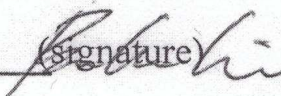
Advisor: Prof. HyunChul Kim

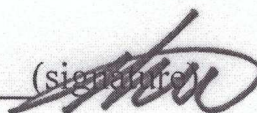
June 2020

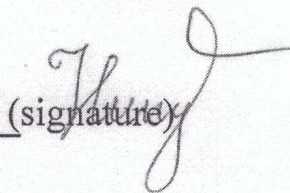
Approved by Committee of the Graduate
School of Inje University in partial
fulfillment of the requirements for the
degree of Doctor of Engineering

Chairman of Committee: Seongbeom Lee (signature) 

Committee: HyunChul Kim (signature) 

Committee: Beomkeum Kim (signature) 

Committee: HyunWoong Seo (signature) 

Committee: Tran Nguyen Hung (signature) 

Graduate School, Inje University

June 2020

Contents

I. INTRODUCTION	1
A. Photovoltaic Energy Conversion	1
1. Solar Cells and Solar Energy Conversion	1
2. Solar Cell Applications	5
B. Perovskite Solar Cells.....	6
1. Crystal Structures of Hybrid Halide Perovskites	7
2. Device Architecture and Materials.....	13
3. Perovskite Solar Cells Fabrication Methods	40
4. Hysteresis Characteristics and Device Stability	43
C. Pulsed Laser Ablation.....	61
1. History of Pulsed Laser Ablation	61
2. Laser for Pulsed Laser Ablation.....	65
3. The Laser Process with Perovskite Solar Cells.....	72
II. PURPOSE OF STUDY	74
III. ENHANCED PERFORMANCE OF PEROVSKITE SOLAR CELLS VIA LASER-INDUCED HEAT TREATMENT	75
A. Materials and Methods	75
1. Laser System	75
2. Methylammonium Iodide (CH ₃ NH ₃ I) Synthesis.....	75
3. Solar Cell Fabrication	76
4. Characterization	77
B. Results and Discussion	77
1. Effects of Laser Operation Parameters on the Grain Size of the Perovskite.....	80

2.	Effects of Laser Operation Parameters on the Photovoltaic Characteristics	83
3.	Simulation of Laser-Induced Heat Treatment	86
4.	Comparison of the Laser-Induced Heat Treatment and Conventional Thermal Heating Process	89
C.	Conclusion	91
IV.	FULLY SOLUTION-PROCESSED PEROVSKITE SOLAR CELLS FABRICATED BY LAMINATION PROCESS	92
A.	Materials and Methods	92
1.	Methylammonium Iodide (CH ₃ NH ₃ I) Synthesis	92
2.	Solar Cell Fabrication	93
3.	Characterization	94
B.	Results and Discussion	95
C.	Conclusion	101
V.	CONCLUSION	102
VI.	List of Research Achievements	104

List of Figures

Figure 1. Solar energy spectra. (a) Data expressed in watts per m ² per 1 nm bandwidth for AMO and for AM1.5G, and AM1.5D spectra and (b) The AM1.5G data expressed in terms of impinging photons per second per cm ² per 20 nm bandwidth.....	2
Figure 2. Cross-section of a typical solar cell	3
Figure 3. The current density-voltage (J-V) characteristic of the photovoltaic structure under illumination.	4
Figure 4: Schematic of the perovskite crystal structure with respect to the A, B and X lattice sites reproduced from Ref. [17].....	9
Figure 5: Temperature dependent (100-352 K) powder neutron diffraction of CH ₃ NH ₃ PbI ₃ from Ref. [22].....	10
Figure 6. Schematic diagram of mesoscopic heterojunction solar cells (a) no perovskite overlayer and (b) with perovskite overlayer; and planar heterojunction solar cells with (c) conventional “n-i-p” and (d) inverted “p-i-n” configurations.	13
Figure 7. Cross-sectional SEM images of FTO/bl-TiO ₂ /mp-Al ₂ O ₃ /perovskite/HTM/Ag solar cells with different thicknesses of the Al ₂ O ₃ scaffold, and the dependence of device parameters on the scaffold thickness [45].	17
Figure 8. Structures of recently reported HTMs for perovskite solar cells.	19
Figure 9. Energy level diagram showing HOMO levels of various HTMs.....	20
Figure 10. Energy level diagram showing conduction band/LUMO levels of various ETLs.....	32
Figure 11. Four general methods for preparing perovskite active layer. (a) Single-step solution deposition, (b) Two-step solution deposition, (c) Thermal vapor deposition, (d) Vapor-assisted solution deposition [135].....	41
Figure 12. Forward and backward scan J-V curves of (a) perovskite (MAPbI ₃) cells of a normal and (b) inverted architecture [139].	44

Figure 13. Forward and backward J-V curves of planar perovskite (MAPBI₃) solar cells of normal architecture with (a) PCBM, (b) TiO₂-PCBM as electron collecting layer and (c) inverted architecture with NiO as hole transport layer [139].....44

Figure 14. Influence of PCBM film thickness on J-V hysteresis of inverted perovskite solar cells. Forward and backward J-V curves of inverted perovskite cell (ITO/PEDOT:PSS/CH₃NH₃PbI_{3-x}Cl_x/PCBM/Al) with PCBM layer of thickness (a) 10 nm, (b) 40 nm and (c) 90 nm [143].....45

Figure 15. An opposite trend of hysteresis (forward scan showing higher performance than reverse scan) observed in an inverted perovskite solar cell. (a) Schematic of the device and (b) J-V curves of forward and reverse scan.....45

Figure 16. Hysteresis changing with cell architecture. Forward bias to short circuit (FB-SC) and short circuit to forward bias (SC-FB) J-V curves of perovskite cell with (a) varying TiO₂ mesoporous thickness (perovskite capping layer increasing with decreasing TiO₂ thickness) and (b) Al₂O₃ scaffold [136].....46

Figure 17. J-V Hysteresis changing with grain size of perovskite. SEM images of CH₃NH₃PbI₃ grown by two-step spin coating method with CH₃NH₃I concentration of (a) 41.94, (b) 52.42, (c) 62.91 mM leading to formation of grains of size 440, 170 and 130 nm. Forward and backward J-V curves of perovskite cells employing the perovskite films with grain size of (d) 440, (e) 170 and (f) 130 nm [146].....47

Figure 18. Current–voltage curves of TiO₂ based CH₃NH₃PbI₃ devices measured with different scan rates from 1 to –1 V and back to 1 V. Sweep rates are from 10 to 100,000 mV s⁻¹ [20]48

Figure 19. (a) Forward and reverse J-V curves of an iodide based perovskite solar cell measured at different temperatures (20, 5, –5 and –15 °C). (b) Forward (dashed line) and reverse (solid line) J-V curves of an inverted perovskite solar cell measured at different temperatures (293, 250, 200, 175 and 77 K)49

Figure 20. Forward scan (FS) and backward scan (BS) J-V curves of (a) Al₂O₃ and (b) planar-structure-based perovskite solar cells under 1 sun illumination. All the cells were applied at various bias voltages in the dark for 5 min before the J-V measurements [154]. 50

Figure 21. Hysteresis loops of $\text{CH}_3\text{NH}_3\text{PbI}_3$ prepared by solution process. A Voltage and b polarization as function of applied bias [28].	52
Figure 22. J-V characteristics of (a) planar heterojunction PbI_2 and (b) $\text{CH}_3\text{NH}_3\text{PbI}_{3-x}\text{Cl}_x$ perovskite solar cells. The measurements were taken under 1 sun illumination (100 mW/cm^2) and at a voltage scan speed of 200 mV/s . Insets represent the corresponding device structures [157]	54
Figure 23. J-V characteristics (voltage scan speed = 200 mV/s) and steady-state performance (measured with an external load of 600Ω) of three planar perovskite cells showing hysteresis of different magnitudes.	56
Figure 24. J-V curves and steady-state current density measured at bias voltages of 0.5 , 0.55 , 0.6 and 0.67 V bias.	57
Figure 25. Laser-focused intensity versus years. The proposed power intensity for the ELI-NP pillar facility at Magurele-Bucharest, Romania is presented [162].	63
Figure 26. The scheme of a Nd-YAG laser.	66
Figure 27. Energetic bands of Ti^{3+} ions in the Al_2O_3 crystal lattice.	69
Figure 28. The simplified schematic diagram of the transition process in an excimer laser with the general features of the transition process.	70
Figure 29. The simplified schematic diagram of the transition processes in a CO_2 laser.	72
Figure 30. The absorption coefficients of perovskite, FTO, and TiO_2 .	78
Figure 31. Graphical illustration of Perovskite film fabrication with (a) conventional method, (b) Laser-induced heat treatment method.	79
Figure 32. Top-view SEM images and grain size distribution of the perovskite corresponding at a defocusing distance of (a) $Z = 0$, (b) $Z = 2 \text{ mm}$, (c) $Z = 4 \text{ mm}$, (d) $Z = 5 \text{ mm}$, and (e) $Z = 6 \text{ mm}$ and (f) on the hot plate at 115°C . Scale bar: $50 \mu\text{m}$ for (a) and $1 \mu\text{m}$ for (b)–(f).	81
Figure 33. Top-view SEM images and grain size distribution of perovskite crystals corresponding to scan speed of (a) 0.5 mm s^{-1} , (b) 1 mm s^{-1} , (c) 1.5 mm s^{-1} .	82

Figure 34. (a) XRD patterns of the perovskite films under different conditions, (b) Relative peak intensity ratio of perovskite (110) lattice plane to PbI_2 (001) lattice plane.	83
Figure 35. (a) UV–vis absorption spectra of perovskite films, (b) J–V characteristics of the cells with the best performing measured by a reverse scan under AM 1.5G conditions.	83
Figure 36. J-V curves of the best performing cells corresponding to various scan speed 0.5, 1, and 1.5 m s^{-1} measured by the reverse scan under AM 1.5G condition.	85
Figure 37. (a) Cross-section of perovskite solar cell, (b) Two-dimensional model of perovskite solar cell for simulation.	86
Figure 38. The prediction of the surface temperature corresponding to (a) various defocusing distances (inset: the laser intensity distribution along with the layers of PSC) and (b) various scan speeds of the laser beam.	89
Figure 39. Top-view SEM images and grain size distribution of perovskite crystals prepared by conventional thermal heating process corresponding to various temperatures (a) 100°C , (b) 115°C , and (c) 130°C	89
Figure 40. J-V curves of the best performing cells prepared by conventional thermal heating process corresponding to various temperatures and measured by the reverse scan under AM 1.5G condition.	90
Figure 41. Hysteresis characteristics of the best PSC of (a) conventional thermal heating process and (b) laser-induced heat treatment.	91
Figure 42. (a) A schematic illustration of lamination process for PSCs fabrication, (b) laminated cell, (c) cross-section image of conventional PSCs, and (d) top-view SEM image of perovskite layer.	95
Figure 43. Variation in sheet resistance of the silver layer with annealing temperature and hold time.	96
Figure 44. The microstructure of silver nanoparticle film annealed at (a) 150°C and (b) 180°C for 5 min.	97

Figure 45. The AFM topographic images of the surface of silver nanoparticle film annealed at 150 °C for different hold time: (a) 2 min, (b) 5 min, (c) 10 min, (d) 15 min, and (e) 20 min. (f) Silver nanoparticle film on a PET substrate.	98
Figure 46. J-V curve of the best performing cells measured by the backward scan at AM 1.5G one sun illumination.....	100
Figure 47. Photovoltaic parameters of the best cells during the study of long-term stability.....	101

List of tables

Table 1. Laser parameters.....	75
Table 2. Laser operation parameters	80
Table 3. The values of the laser fluence corresponding to defocusing distances ...	80
Table 4. Average performance parameters of PSCs.....	85
Table 5. Simulation parameters.....	86
Table 6. Nomenclature	88
Table 7. Average performance parameters of nine cells with conventional and laminated methods.	100
Table 8. J-V parameters of the best cells before and after 28 days	101

Acknowledgements

Foremost, I would like to express my deep gratitude to my supervisor Prof. Hyun Chul Kim for thoughtful guiding and supporting throughout my Doctor course. I really appreciate the extensive knowledge and inspiration he has given to me, which help me to complete my work. I would also like to express my deep appreciation to the thesis committee members; your comments and feedback are truly valuable.

Beside my supervisor, I would like to thank Prof. Hyun Woong Seo and Dr. Thuy Thi Cao for their insightful comments and hard questions while I do experiment and revise papers.

I am grateful to Lab members for their helps during my academic life at the Inje University. Thank you for sharing your knowledge and expertise with me.

I am very much thankful to my friends in Korea, who share with me happiness, sadness, and warm memories during the period of Doctor study. Especially, many thanks to Dr. Thuy Thi Cao, Mr. Hoang Huu Trung, Ms. Dang Thi Hong Nhung, and Mr. Thien Thanh Dao, for the devoted giving me inspiration to release stresses at research and overcome obstacles in life. Thank you all for being a piece of my life, always beside to encourage and make me less homesick.

I also want to thank the staffs of the Graduate School and Department of Mechanical Engineering for assisting me in official documents and giving me chances to understand Korean culture.

Last but not the least, I would like to express my very profound gratitude to my family and to my wife for providing me with unfailing support and continuous encouragement throughout my years of study and through the process of researching and writing this thesis. This accomplishment would not have been possible without them. Thank you.

ABSTRACT

Study on the Improvement of Perovskite Solar Cell Efficiency

Trinh Xuan Long

(Advisor: Prof. HyunChul Kim, Ph.D.)

Department of Mechanical Engineering

Graduate School, Inje University

Perovskite solar cells have recently attracted a great attention because they have shown excellent photovoltaic performance, obtainable via a facile and cheap process. In the last decade, perovskite solar cells based on methylammonium lead halides have shown exceptional progress in terms of power conversion efficiency. The device performance highly depends on the film morphology and the film morphology is influenced by factors such as the material composition, additives, film treatment and deposition method. The key to obtaining high quality film morphology and performance is to essentially lower the energy barrier for nucleation and to form uniform growth of the perovskite crystals. In this work, we present a versatile laser-induced heat treatment, which can be used to control the morphology and grain size of perovskite and hence improving the PCE of PSCs. The structure of PSC devices is as follows: FTO glass substrate/compact (TiO₂)/mesoporous (TiO₂)/perovskite CH₃NH₃PbI₃/Spiro-MeOTAD/silver film. A nanosecond-pulsed ytterbium-doped fiber laser with a wavelength of 1064 nm was used to induce local heating on a perovskite film after the reaction between methyl ammonium iodide (MAI) and lead iodide (PbI₂) was completed. The laser operation parameters, such as the defocusing distance and scan speed, were investigated to control the grain size of the perovskite.

Based on optimized laser operation parameters, the best and average PCEs of 13.03% and $12.45 \pm 0.28\%$, respectively, were achieved, which are higher than those obtained with conventional thermal heating (the best and average PCEs of 11.43% and $10.98 \pm 0.25\%$, respectively). A perovskite layer temperature of 115°C was predicted by simulating the energy absorption of the perovskite film under optimized laser operation conditions using COMSOL software.

Beside, we also report a fully solution-processed fabrication of perovskite solar cell using silver nanoparticle film as the top electrode by lamination. The lamination process is an excellent alternative to replace vacuum deposition method due to its low cost, ease of processing, and potential to scale-up. The configuration of perovskite solar cell is FTO/cp-TiO₂/mp-TiO₂/CH₃NH₃PbI₃/Spiro-MeOTAD/PEDOT:PSS/D-sorbitol/silver nanoparticle film. The silver nanoparticle film was produced by spin-coating the nanoparticle silver ink onto a poly(ethylene terephthalate) (PET) substrate followed by post-annealing at 150 °C for 5 min. Introduction of a thin layer of Poly(3,4-ethylenedioxythiophene) polystyrene sulfonate PEDOT:PSS/D-sorbitol, plays an important role in improving the adherence of devices and electrical contact during lamination. Thereby, laminated perovskite solar cells with average power conversion efficiency (PCE) of 10.03% were achieved, almost of 90% of the PCE obtained for conventional devices (11.19%) with evaporated silver contact. The electrical and morphological properties of thermally annealed silver nanoparticle film were also investigated.

Keywords: Perovskite solar cells, two-step solution deposition, laser-induced heat treatment, simulation, COMSOL software, lamination method, silver nanoparticle film.